Free-Surface Elevation due to Moving Pressure Distributions in Three Dimensions

D. C. Scullen and E. O. Tuck

Department of Applied Mathematics
The University of Adelaide, Australia 5005.

March 23, 2001

Abstract

Efficient and accurate code is described for computation of the free-surface disturbance of a travelling pressure distribution. Near-field and far-field results are given for constant-pressure rectangular patches, and for non-uniform pressure distributions, including examples with both smooth and singular edge behaviour.

1 Introduction

The aim of the present paper is to describe and illustrate a computational procedure for determining the shape $z = Z(x, y)$ of the disturbance to the otherwise-plane free surface $z = 0$ of a body of water of infinite depth, due to passage at uniform speed U of a pressure distribution having a small prescribed excess $p(x, y)$ over atmospheric. This fully three-dimensional wave field can be determined with high accuracy everywhere, namely around, under, near to, or far from the pressure disturbance.

There are obvious direct applications, to travelling meteorological disturbances or to hovercraft, for example. In addition, there are indirect or inverse potential applications, where one may seek to determine the pressure distribution $p(x, y)$ in order to produce a specified disturbance $Z(x, y)$ within

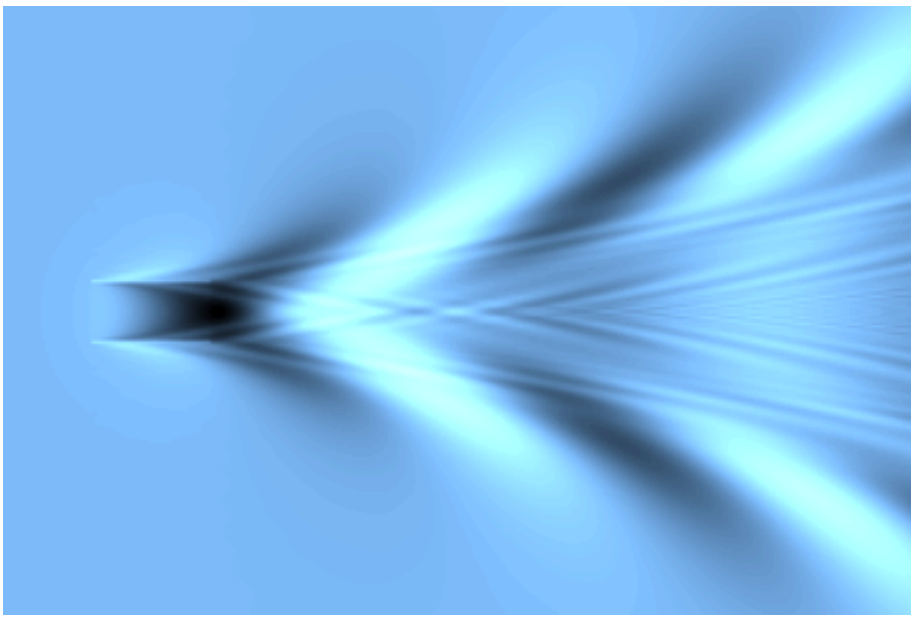

Figure 1: Contour plot of surface elevation due to constant-pressure patch.

some portion of the plane $z = 0$. This is the topic of "flat-ship" theory, and is related to planing. Although we shall not consider such inverse problems in the present paper, the algorithms produced here for the direct problem may serve as the basis for solution of the inverse problem.

The analytic relationship between the input $p(x, y)$ and the output $Z(x, y)$ is well known (see e.g. Wehausen and Laitone [12]), and involves a quadruple integration, namely integrals with respect to both spatial co-ordinates and with respect to the wavenumber and direction of the waves. The fact that this task involves four numerical integrations, some of which are inherently of significant computational complexity (specifically for example due to the need to cope with rapidly-oscillating integrands), has meant that only a few detailed three-dimensional computations have been attempted in the past, at least in the near field of the disturbance. Some examples are in [4], [2] and [3].

It is possible to decompose the flow and hence the wave elevation Z into the sum of two components that represent respectively the (wave-less) local and (wave-like) far-field behaviour. Although the terminology "local" and "far-field" will be used to describe these components, each of them must

be evaluated at every point of the desired field of observation. It is true, however, that the local component decays quite rapidly as we move away from the disturbance.

The local component, which remains a quadruple integral, can nevertheless be handled efficiently in a manner described by Newman [6], which effectively eliminates the wavenumber and wave-direction integrals, so reducing its complexity to that of a double spatial integral. The far-field component, by comparison, is a triple integral which can be handled efficiently for computations over a large grid by first performing a once-only double spatial integration, followed by a single wave-direction integration which must be performed separately for each required field point. This last integration (with rapidly varying integrand) is difficult and computationally expensive, but we use acceleration techniques that have been tested in other contexts, to produce results of about 4-figure accuracy in reasonable computer times.

In the present paper, all computations are performed for pressures that are non-zero only on a rectangular patch with beam/length ratio 0.5, travelling at a length-based Froude number of $1/\sqrt{2} \approx 0.7$. We describe how the full wave elevations can be obtained for any input pressure distribution $p(x, y)$.

We first give detailed results for a pressure $p(x, y) = p_0$ which is constant over the rectangular patch. For this case, we can also provide an independent check, as the spatial integrations can be done analytically, and the wavenumber integration can be reduced to evaluation of sine and cosine integrals, for which there are rapid codes. Thus essentially only a wave-direction integration need be performed. Having verified good agreement between this special result and the output of our general-purpose code, we display detailed wave fields, including observation points close to the corners and edges of the patch.

Figure 1 shows a contour plot of the surface elevations produced by the constant-pressure patch in a domain that extends aft of the patch for several wavelengths. The surface elevation has been determined at each point of a 301x301 grid (more than 90,000 points) in less than 15 minutes using a single processor of a 20-cpu SGI Power Challenge. Approximately 100 surface elevations are evaluated each second. Similar speeds can be achieved on a 650MHz Pentium III PC.

We then consider various examples of non-uniform pressure distributions $p(x, y)$, including a doubly-elliptical variation, where the edge behaviour is smoother than that for constant pressure. This particular distribution in

fact makes *larger* far-field waves than does a constant-pressure patch with the same net lift, having a wave resistance about 1.4 times as high at Froude number 0.7. We also consider an example of a tandem-patch pressure distribution (again with the same net lift on the same rectangular domain) which makes *smaller* waves, having a wave resistance only about half of that of the constant-pressure patch. Finally, we consider an unbounded pressure distribution, with an inverse square-root singularity at the leading edge. Although the program is not specifically designed to cope with such pressures, it nevertheless gives good results, with leading-edge behaviour characteristic of the linearised representation of the spray-root zone of a planing surface.

2 Pressure points and surface sources

The velocity potential for the flow induced by a unit delta-function pressure [12, page 598] exerted on the free surface of a stream U is proportional to G_x, where $G(x, y, z)$ is the velocity potential for a unit ("Havelock") source located at the free surface [12, page 484], namely in infinite water depth

$$G(x,y,z) = \frac{k_0}{2\pi^2} \Re \int_{-\pi/2}^{\pi/2} d\theta \sec^2\theta \int_0^\infty dk\, e^{-ik(x\cos\theta + y\sin\theta)+kz} \frac{1}{k - k_0 \sec^2\theta}\ . \tag{1}$$

The path of k-integration in (1) passes above the pole at $k = k_0 \sec^2\theta$, with $z \le 0$ and $k_0 = g/U^2$.

That is, a pressure point is a surface horizontal dipole. The velocity potential of a distribution of pressure $p(x, y)$ over a region B of the plane $z = 0$ is then

$$\phi(x,y,z) = \frac{U}{\rho g} \iint_B d\xi d\eta\ p(\xi,\eta)\ G_x(x-\xi, y-\eta, z). \tag{2}$$

Thus, for any given pressure $p(x, y)$, the potential $\phi(x, y, z)$ is given by a quadruple integral (with respect to ξ, η, k, θ), and one can expect its evaluation to be computationally expensive.

To obtain the actual wave elevation $z = Z(x, y)$ we can proceed either by x-integration of the kinematic condition $\phi_z = UZ_x$, giving

$$Z(x,y) = \frac{1}{\rho g} \iint_B d\xi d\eta\ p(\xi,\eta)\ G_z(x-\xi, y-\eta, 0), \tag{3}$$

or by use of the dynamic condition $p/\rho + gZ + U\phi_x = 0$, to give

$$Z(x,y) = -\frac{p(x,y)}{\rho g} - \frac{1}{\rho g k_0}\iint_B d\xi d\eta\; p(\xi,\eta)\; G_{xx}(x-\xi, y-\eta, 0). \quad (4)$$

The two forms (3) and (4) can be shown to be equivalent, noting that the first term in (4) is the hydrostatic displacement due to the given pressure $p(x,y)$.

3 Local and far-field decompositions

The local-far decomposition for the actual Green's function can be written

$$G(x,y,z) = G^L(x,y,z) + G^F(x,y,z) \quad (5)$$

where (with the path of integration now diverted below the pole)

$$G^L(x,y,z) = \frac{k_0}{2\pi^2}\Re\int_{\pi/2}^{\pi/2} d\theta \sec^2\theta \int_0^\infty dk \frac{e^{-ik(|x|\cos\theta + y\sin\theta)+kz}}{k - k_0\sec^2\theta} \quad (6)$$

and

$$G^F(x,y,z) = -\frac{k_0}{\pi}H(x)\Re i\int_{\pi/2}^{\pi/2} d\theta \sec^2\theta e^{-ik_0\sec^2\theta(x\cos\theta + y\sin\theta)+k_0 z\sec^2\theta}. \quad (7)$$

The quantity G^L (which is an even function of x and tends to zero rapidly as $|x| \to \infty$) is that for which rapidly-computable 6-figure accurate polynomial approximations due to Newman [6] are available. Newman in fact gave tables of values and associated formulae only for G^L itself, but it is possible to determine corresponding formulae for the derivatives of G^L that are required in the present application.

In the representation (7) for the far-field potential G^F, the quantity $H(x)$ is the Heaviside unit step function, i.e. $H = 0$ for $x < 0$ and $H = 1$ for $x > 0$. Thus the potential G^F vanishes identically ahead of the point disturbance, and for pressure points distributed over a region B, at each fixed x value only those pressure points located at points (ξ,η) ahead of the point of observation (x,y) can contribute.

Thus, writing $\phi = \phi^L + \phi^F$ to represent the local and far-field components of the potential, we have

$$\phi^L(x,y,z) = \frac{U}{\rho g}\iint_B d\xi d\eta\; p(\xi,\eta)\; G^L_x(x-\xi, y-\eta, z) \quad (8)$$

and

$$\phi^F(x,y,z) = -\frac{U}{\rho g}\frac{k_0^2}{\pi}\Re\int_{-\pi/2}^{\pi/2} d\theta \sec^3\theta e^{-ik_0(x\sec\theta + y\sec^2\theta\sin\theta) + k_0 z\sec^2\theta}(P+iQ) \tag{9}$$

where

$$P + iQ = \iint_B d\xi d\eta\; p(\xi,\eta)\; e^{ik_0(\xi\sec\theta+\eta\sec^2\theta\sin\theta)}\; H(x-\xi)\;. \tag{10}$$

In general, $P = P(x,\theta)$ and $Q = Q(x,\theta)$, i.e. these functions must be computed and stored separately not just for each wave-propagation angle θ, but also for each value of the co-ordinate x (but not y). However, as is clear from the properties of the Heaviside function $H(x-\xi)$, they vanish entirely for all points ahead of the pressure region B and are independent of x for all points astern of B.

When differentiating the far-field potential with respect to x, care must be taken to ensure that the dependence of $P + iQ$ on x is accounted for. This dependence creates, for a pressure patch with non-zero pressure at the leading or trailing edge, a discontinuity in the far-field elevation at and to the sides of that edge. However, a discontinuity of equal magnitude but opposite sign occurs in the local-field elevation, so that the resulting total free surface is continuous.

In previous work on thin ships [8], we have developed techniques for fast and accurate evaluation of integrals of rapidly oscillating functions similar to (9). We have found that Filon quadrature accurately captures the oscillatory nature of (10) and, when combined in the far field with the pseudo-stationary-phase algorithm described by Tuck *et al* [10], enables accurate evaluation of (9) and its derivatives everywhere in reasonable computer times.

Some difficulties are encountered when determining the local component ϕ^L and its derivatives on the free surface directly beneath the pressure patch, since G_x^L and its derivatives are singular at the origin. For the surface elevation, the integral involves G_{xx}^L which is singular and an even function of x, and thus the integral is divergent; formally a Hadamard interpretation is required. Nevertheless, these difficulties can be overcome to produce the potential and its derivatives accurately everywhere within the fluid domain, including directly beneath the region of applied pressure.

4 Constant-pressure rectangular patch

If $p(x,y) = p_0 =$ constant, and B is the rectangle $|x| < a, |y| < b$, then the expression (3) gives

$$\begin{aligned} Z(x,y) &= \frac{p_0}{\rho g} \iint_B d\xi d\eta \; G_z(x-\xi, y-\eta, 0) \\ &= \frac{p_0}{\rho g}\Big[Z^0(x-a,y-b) - Z^0(x+a,y-b) \\ &\qquad\qquad -Z^0(x-a,y+b) + Z^0(x+a,y+b)\Big] \end{aligned} \tag{11}$$

where

$$Z^0_{xy}(x,y) = G_z(x,y,0). \tag{12}$$

Hence

$$Z^0(x,y) = -\frac{1}{2\pi^2}\Re \int_{-\pi/2}^{\pi/2} \frac{d\theta}{\sin\theta\cos\theta} \int_0^\infty e^{-ik(x\cos\theta + y\sin\theta)} \frac{k_0 \sec^2\theta}{k - k_0\sec^2\theta}\,\frac{dk}{k} \tag{13}$$

$$= -\frac{1}{2\pi^2}\Re \int_{-\pi/2}^{\pi/2} \frac{d\theta}{\sin\theta\cos\theta} \int_0^\infty e^{-ik(x\cos\theta + y\sin\theta)} \frac{dk}{k - k_0\sec^2\theta} - \frac{1}{4}\,\mathrm{sgn}(x)\,\mathrm{sgn}(y)\;. \tag{14}$$

That is, the wave elevation (11) due to a constant-pressure rectangular patch requires only four evaluations (at the four corners of the rectangle) of the single special function $Z^0(x,y)$. Note that Z^0 is non-dimensional and the wave number k_0 can be scaled with the co-ordinates (x,y), so in effect in its evaluation we can set $k_0 = 1$. Physically, $z = Z^0(x,y)$ is the surface elevation due to a pressure distribution of the form

$$p(x,y) = \frac{1}{4}\,\mathrm{sgn}(x)\,\mathrm{sgn}(y)\;, \tag{15}$$

the corresponding (negative) term in (14) being the non-dimensional hydrostatic depression due to this pressure.

The k-integral in (13) or (14) can be expressed in terms of sine and cosine integrals, with (13) leading to

$$Z^0(x,y) = -\frac{1}{2\pi^2}\int_{-\pi/2}^{\pi/2} \frac{g(T) + \log|T| - 2\pi H(T)\sin T}{\sin\theta\cos\theta}\,d\theta \tag{16}$$

where $T = k_0 x \sec\theta + k_0 y \sec^2\theta \sin\theta$, and $g(T)$ is the even auxiliary function for the sine and cosine integrals ([1], p. 232). The term in $\log|T|$ just contributes the hydrostatic depression in (14), but it is computationally preferable to retain it as part of the θ-integrand, as it cancels a corresponding singularity in $g(T)$.

The corresponding split $Z^0 = Z^L + Z^F$ into local and far-field components respectively is

$$Z^L(x,y) = -\frac{1}{2\pi^2}\int_{-\pi/2}^{\pi/2} \frac{g(T) + \log|T| - 2\pi[H(T) - H(x)]\sin T}{\sin\theta\cos\theta}\, d\theta \qquad (17)$$

and

$$Z^F(x,y) = \frac{H(x)}{\pi}\int_{-\pi/2}^{\pi/2} \frac{\sin T}{\sin\theta\cos\theta}\, d\theta. \qquad (18)$$

The task of computing the wave elevation due to a constant-pressure rectangular patch can thus be reduced to that of a single integral with respect to wave angle θ, the integrand being a combination of sine and cosine integrals and trigonometric functions. The former are efficiently computable, e.g. by polynomial representations as in [1], page 233. The latter terms present more difficulty, as they are rapidly oscillating when $|\theta| \to \pi/2$, but this is tractable (e.g. by using an artificial viscosity factor) and 4-figure accuracy is obtainable with about 20,000 points in Simpson's rule.

The results of computations based on the present section then agree everywhere to at least 4 significant figures with those of our general purpose code to be discussed in the following section. A further check is that the net wave resistance agrees with that given by Newman and Poole [7] and others. Also, using our general purpose code we have been able to reproduce the surface elevations shown in Huang and Wong's [4] Figure 2 and Cheng and Wellicome's [2] Figure 3. The latter includes elevations for a pressure distribution that varies sinusoidally in the transverse direction. Further, Lamb's two-dimensional result ([5], page 404) is reproduced along the centreline of rectangles with large b/a ratios. Notably, the leading and trailing-edge slopes tend to infinity in this limit, but remain finite for all finite b/a.

Figure 2 shows the resulting surface elevations produced by such a constant-pressure rectangular patch. There is no restriction on the grid spacing used within our program, but for the purposes of clarity we use a coarse grid for the mesh plots. Much finer resolution is used for the contour plots. The particular case under investigation has $k_0 a = 1$ with $b/a = 0.5$. Perhaps surprisingly, in spite of the step-function character to the pressure, there are no

discontinuities in the free surface at the leading and trailing edges, although step discontinuities are present along the sides of the patch.

To interpret this behaviour, it is instructive to plot the far-field and local-field components separately. Figure 3 shows the breakdown into (a) far-field and (b) local-field components, whose sum is (c) the total elevation. For clarity, only the region $y > 0$ is shown.

The plot of the far-field surface elevation (a) shows a discontinuity at the leading and trailing edges, not just within the pressure patch, but also at y values outside the patch. The magnitude of this discontinuity is greatest within the patch, undergoes a step jump at the patch corners, and then continues indefinitely to the sides, with a slow decay with respect to y. There is a transverse wave directly beneath the pressure patch, its character being most obvious along the centreline of the patch. In addition, radiating from the leading corner of the region is a Kelvin-like wave pattern, much like the usual far-field wave pattern for a ship, except that here it is antisymmetric in the y-direction. Although less clearly visible, a similar disturbance emanates from the trailing corner. The surface elevation is continuous in the y-direction everywhere except at the corners of the patch, where the y-slope becomes infinite. Away from the corner, the y-slope diminishes rapidly. The limiting value of the x-derivative of the far-field surface elevation is zero as the leading edge is approached from within the patch, so the slope is continuous there. Similarly, the slope is finite and continuous across the trailing edge.

The dominant feature of the local field (b) is the depression corresponding to the hydrostatic pressure experienced directly beneath the patch. Without this hydrostatic depression, the local field would be continuous in the y-direction for all values of x, and of relatively small magnitude everywhere, decreasing rapidly in all directions. There is a discontinuity in the local elevation at and to the sides of the leading and trailing edges, the magnitude of which exactly cancels the corresponding discontinuity in the far-field component. The x-derivative of the local surface elevation is finite and continuous everywhere.

The total wave elevation (c) obtained by summing (a) and (b) is then continuous with continuous finite slope across the leading and trailing edges, both inside and outside the patch, for all y except at the actual corner points. Along the sides of the patch, the surface elevation is a discontinuous function of y, for all x within the patch length, the step jump having the hydrostatic magnitude $p_0/\rho g$. Otherwise, the elevation and its slope in every direction are continuous everywhere.

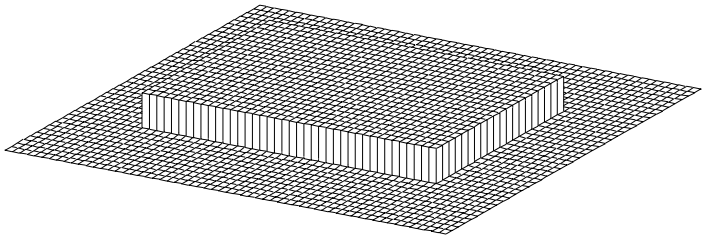

(a) Pressure distribution

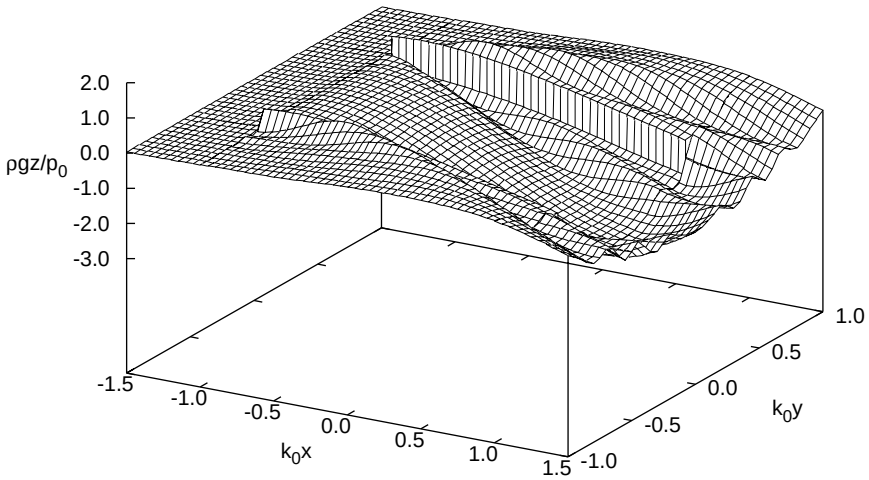

(b) Free surface

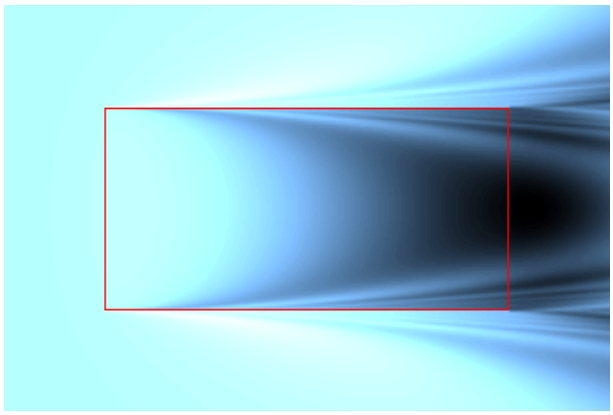

(c) Contour plot of free surface

Figure 2: Surface produced by a constant-pressure rectangular patch such that $k_0 a = 1$, $b/a = 0.5$.

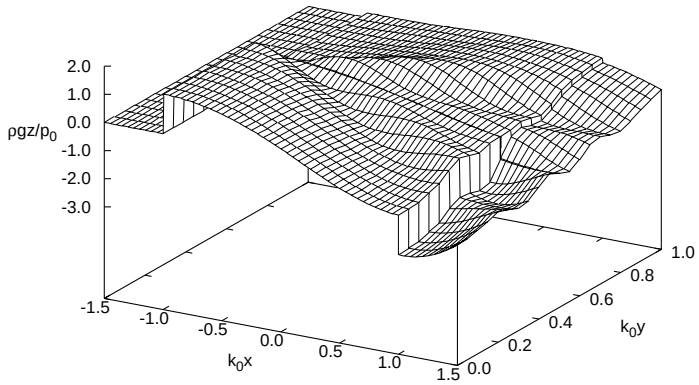

(a) Far-field component

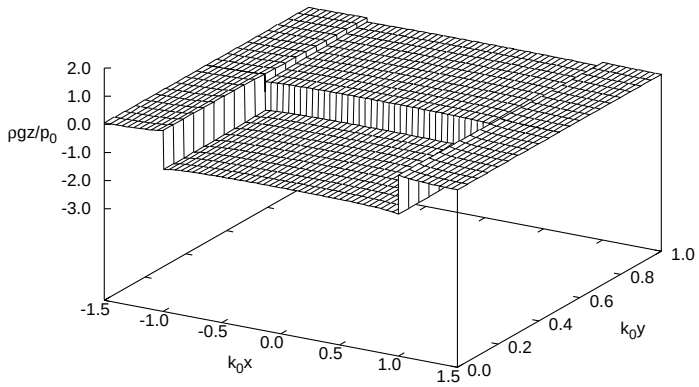

(b) Local-field component

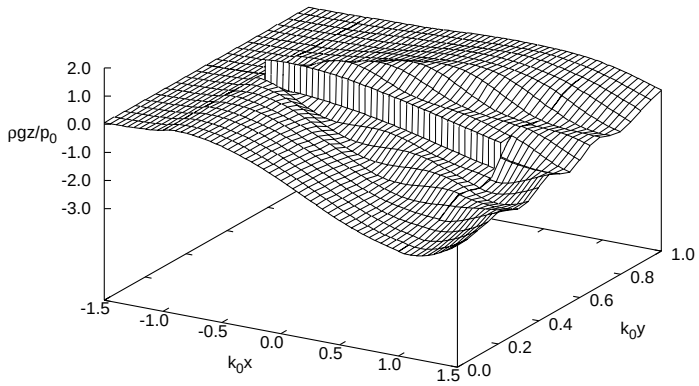

(c) Total wave elevation

Figure 3: Surface-elevation components for the constant pressure distribution.

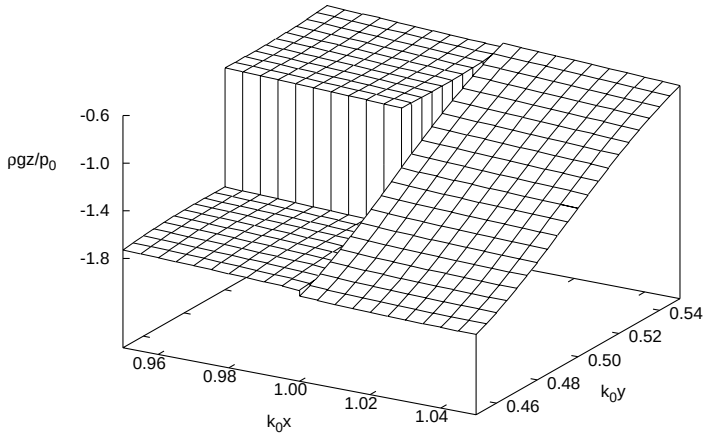

(a) $\Delta\theta = \pi/4096$

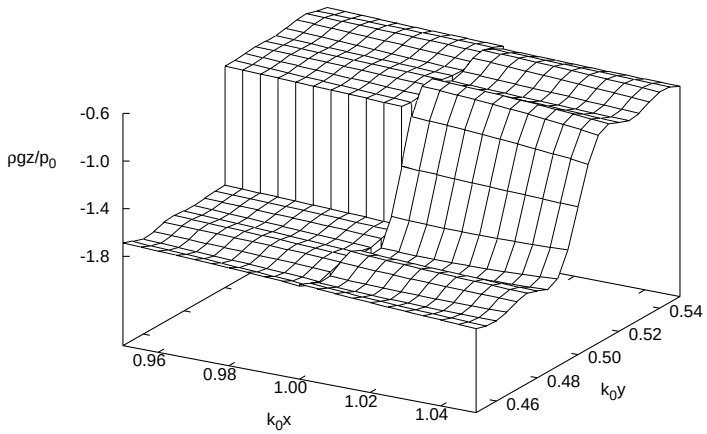

(b) $\Delta\theta = \pi/65536$

Figure 4: Surface elevation near the rear right corner of a step pressure as determined by the numerical method. Behaviour similar to Gibbs phenomenon is observed.

Since this applied pressure distribution is non-zero at its boundaries, it is particularly difficult to determine accurately the flow near its corners. Figure 4 shows a magnified view of the surface elevation at the rear right corner of Figure 3 (c). In the top subfigure (a), the far-field θ-integration has been numerically approximated using 4096 subintervals (the same as in Figure 3), whereas a much finer grid of 65536 subintervals has been used for subfigure (b). It is clear that the local mismatch in the surface elevation along the trailing edge is due to numerical error in the far-field calculation. As we approach the corner from astern (increasing x), the far-field surface elevation must remain continuous in all directions until we actually reach the corner itself, at which point a step discontinuity in the lateral y direction must appear instantly. Ideally, the far-field surface should be represented by a continuous integral of plane waves propagating at all angles θ, but in practice the integral is discretised to a sum over a finite number of angles, from which a numerical error results. This is similar to Gibbs phenomenon, which occurs when approximating a step jump using truncated Fourier series. A similar difficulty is encountered at the leading corners. Although this difficulty is reduced by using a very large number of subintervals of θ (as in part (b) of Figure 4), it is only necessary to do this at points very close to the corners.

5 Computational procedure for non-uniform pressure

We concentrate now on determining the free-surface elevation, especially the local component, directly beneath or close to a rectangular region of applied non-uniform pressure. The far-field component can be determined everywhere as described earlier for any pressure distribution, and similarly there is no difficulty in direct computation of the local component at points not close to the pressure patch. Although the local component is not wave-like and does not require integration of rapidly-varying integrands, it does require integration of a distribution of pressure points, and the integrand is highly singular near the location of each such pressure point. This singularity must be treated carefully to ensure good accuracy.

Suppose first we subtract off the hydrostatic pressure and write

$$Z^L(x,y) = -\frac{p(x,y)}{\rho g} - \frac{U^2}{\rho g^2} Z_1(x,y) \tag{19}$$

where

$$\begin{aligned} Z_1(x,y) &= \iint_B d\xi d\eta\; p(\xi,\eta)\; G^L_{xx}(x-\xi, y-\eta, 0) \\ &= \int d\eta \int d\xi\; [p(\xi,\eta) - p(x,\eta)]\, G^L_{xx}(x-\xi, y-\eta, 0) \\ &\quad + Z_2(x-a,y) - Z_2(x+a,y) \end{aligned} \tag{20}$$

with

$$Z_2(x,y) = -\int d\eta\, p(x,\eta) G^L_x(x, y-\eta, 0). \tag{21}$$

In the first term of (20) we have subtracted the pressure at location (x,η), so that the ξ-integration now is non-singular and this double integral can be evaluated by Simpson's rule with respect to both ξ and η.

The remaining terms $Z_2(x-a,y) - Z_2(x+a,y)$ of (20) correct for this subtraction, but now the ξ-integration is explicit, and to evaluate $Z_2(x,y)$ we only have to do a single integration with respect to η. However, again the kernel of this integral is singular at $\eta = y$ when $x = 0$. This singularity thus manifests itself at the leading and trailing edges $x = \pm a$, and it is our aim to maintain consistent accuracy near such points. Hence again we subtract and add $p(x,y)$ to give

$$Z_2(x,y) = -\int d\eta\; [p(x,\eta) - p(x,y)]\, G^L_x(x, y-\eta, 0) + p(x,y) Z_3(x,y) \tag{22}$$

where

$$Z_3(x,y) = -\int d\eta\, G^L_x(x, y-\eta, 0). \tag{23}$$

Ideally the η-integral in (23) would be performed explicitly, and this could be done if suitable polynomial approximations were available as in [6]. However, for the present purpose it is sufficient to carry out this integral numerically, provided yet again we remove the most singular part, writing

$$Z_3(x,y) = -\int d\eta\; \left[G^L_x(x, y-\eta, 0) - F_y(x, y-\eta)\right] - \int d\eta\, F_y(x, y-\eta) \tag{24}$$

where $F_y(x,y)$ models the small-argument behaviour of $G^L_x(x,y,0)$, namely

$$F_y(x,y) = \mathrm{sgn}(x) \frac{k_0^2}{4\pi} \left[\log \frac{k_0(r+|x|)}{4} + \frac{|x|}{r+|x|} + \gamma\right] \tag{25}$$

where γ is Euler's constant, and $r = \sqrt{x^2 + y^2}$. The appropriate y-antiderivative of F_y is

$$F(x,y) = \mathrm{sgn}(x)\mathrm{sgn}(y)\frac{k_0}{4\pi}\left[k_0|y|\left(\log\frac{k_0(r+|x|)}{4} + \gamma - 1\right) + 2k_0|x|\log k_0(r+|y|) - \frac{k_0|x||y|}{r+|x|}\right]. \quad (26)$$

Since F_y is discontinuous at $y = 0$, care is required when performing the last integral in (24) if $y < |b|$. This small-argument behaviour of G^L_x can be found by differentiating the local-field component of Newman's [6] equation (11) and completing an analysis similar to that of his Section 3. It is essentially the small-k_0 limit of G_x, and as such is closely related to the xxy-antiderivative of the kernel of the aerodynamic lifting-surface equation given by Tuck ([9], equation (1.5)).

This particular formulation has the desirable property that all of the integrands are zero at $(\xi, \eta) = (x, y)$ and small nearby, so that they can be computed numerically, even though G^L_{xx} and G^L_x are singular there. Without such a desingularisation, the integrals cannot be determined accurately by numerical means.

Although at points external to the region of applied pressure the derivatives of G^L are not singular, they can be large, especially if the field point is near the edge of the region. Then, the appropriate corrections are based on the pressure at the edge of the region. For example, for a point just ahead of the leading edge, one should replace $p(x, \eta)$ by $p(-a, \eta)$ and $p(x, y)$ by $p(-a, y)$. Again all integrands are well behaved, and the integrals can be determined accurately by Simpson's rule.

Also note that if $p(x, y) = p_0$ is constant, all terms involving subtracted pressures are zero and the surface elevation for a constant-pressure patch is just obtained from Z_3, so that the ability to accurately determine the surface elevations due to a constant-pressure patch is fundamental to the desingularisation process. This connection to the constant-pressure case is emphasised by noting that (apart from the hydrostatic terms) the quantity Z_3 defined in (23) can be expressed in terms of differences of the local part Z^L defined in (17) of the function Z^0 used in the previous section, namely

$$Z_3(x,y) = -k_0\left[Z^L(x, y-b) - Z^L(x, y+b)\right]. \quad (27)$$

6 Results for non-uniform pressures

As a first application for non-uniform pressure, Figure 5 shows the surface elevations produced by a bi-elliptic pressure distribution

$$p(x,y) = p_1 \sqrt{\left(1 - \frac{x^2}{a^2}\right)\left(1 - \frac{y^2}{b^2}\right)}, \tag{28}$$

with $k_0 a = 1$, $b/a = 0.5$, and $p_1 = (16/\pi^2)p_0 =$ constant. With this choice of p_1, the net lift or integral of the pressure takes the same value as that for a constant-pressure patch with pressure p_0. Immediately noticeable is the lack of any step discontinuities in the elevation, which is to be expected since the applied pressure now vanishes at each edge of the region.

Figure 6 shows the breakdown into (a) far-field and (b) local components, compared with (c) the total elevation. The far-field component is now continuous, although it has discontinuous slope in the x-direction at the leading and trailing edges due to the non-zero slope of the pressure there. The local component is again dominated by the hydrostatic depression corresponding to the applied pressure, and therefore is continuous everywhere but with discontinuous x-slope at the leading and trailing edges, and discontinuous y-slope at the right-hand edge of the region. The discontinuities in the x-slope of the separate far-field and local components at the leading and trailing edges cancel each other, so that the total free-surface elevation is continuous everywhere, with continuous slope everywhere except in the y-direction at the edges of the patch. This particular pressure distribution has a wave resistance which is approximately 42% more than that of a constant-pressure rectangular patch with the same net lift; smoothing of the edges of the pressure distribution does not necessarily reduce the size of the far-field waves generated.

As a further example of a non-uniform pressure distribution on the rectangular domain $|x/a| < 1, |y/b| < 1$, consider

$$p(x,y) = \begin{cases} 0 & |x/a| < 0.428, \\ p_1\,[1 - (y/b)^2] & 0.428 < |x/a| < 1 \end{cases} \tag{29}$$

where $p_1 = 2.622 p_0$. This corresponds to two separate pressure distributions in tandem, each pressure being constant in the x-direction, while varying parabolically in the y direction. This configuration, including the choice of the central void as 42.8% of the length, was arrived at by trial and error as one

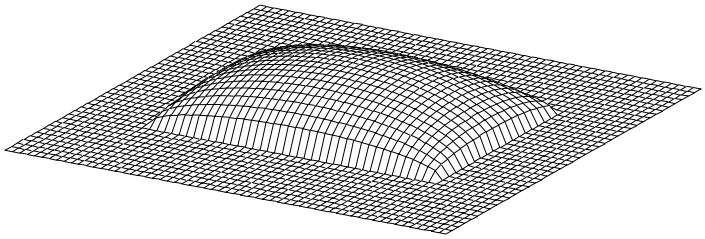

(a) Pressure distribution

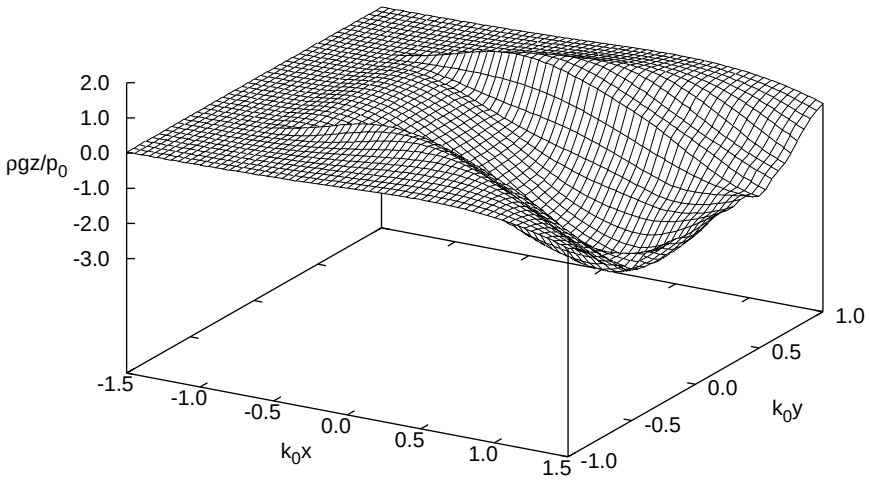

(b) Free surface

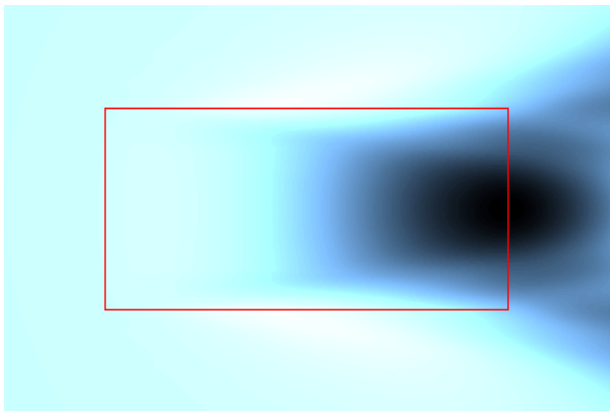

(c) Contour plot of free surface

Figure 5: Surface produced by a bi-elliptic pressure distribution over a rectangular patch such that $k_0 a = 1$ with $b/a = 0.5$.

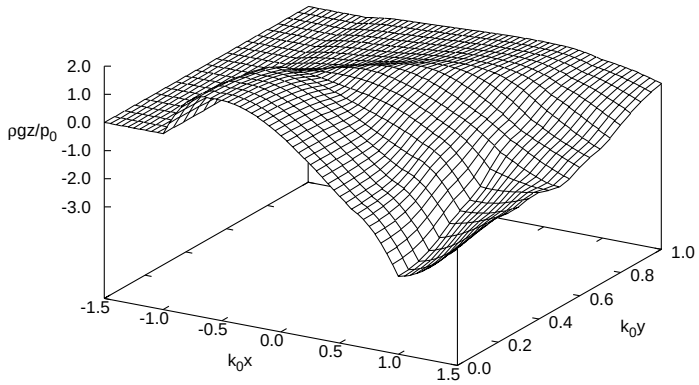

(a) Far-field component

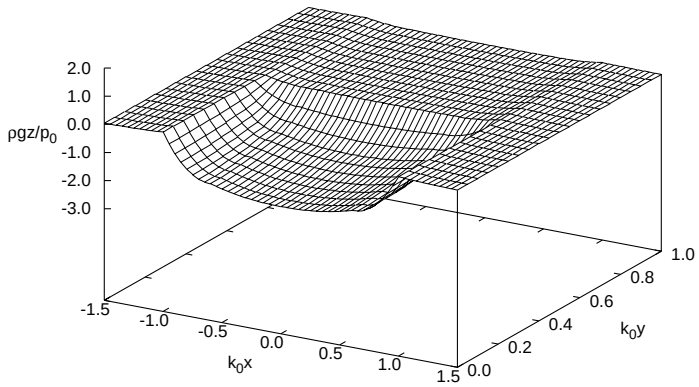

(b) Local-field component

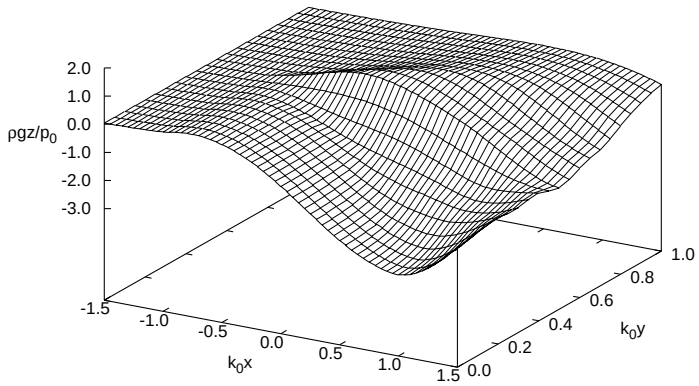

(c) Total wave elevation

Figure 6: Surface-elevation components for the bi-elliptic pressure distribution.

having low wavemaking characteristics, with a wave resistance at $F = 1/\sqrt{2}$ that is only 55% of that for a constant pressure having the same net lift. A more systematic search for pressure distributions with low wave resistance is reported elsewhere [11]. Figure 7 shows the resulting free-surface elevations in the region around the patch. A planing hull of small draft whose hull shape was of the form plotted in this Figure would, subject to the assumptions of the theory, at this speed produce the same pressure distribution and hence free-surface elevation, wave resistance and lift.

It is not our intention here to determine the pressure distribution and free-surface elevation resulting from flow about a planing hull of specified shape. However, that class of problems is important, and it is interesting to see how well the present program might handle pressure distributions typical of those exerted on a given hull surface of small draft. We anticipate the greatest difficulty with the spray-root singularity which is encountered at the leading edge for most flat-bottomed planing boats. We approximate such a case with an applied pressure distribution of the form

$$p(x,y) = p_1 \sqrt{\frac{1-x/a}{1+x/a}\left(1-\frac{y^2}{b^2}\right)} \tag{30}$$

which has the required general nature, namely an inverse-square-root singularity at the leading edge $x = -a$, and a square-root vanishing behaviour at the trailing edge $x = +a$ and sides $y = \pm b$. Since the current program cannot input an infinite pressure, we modify the input so that the pressure at the actual leading edge $x = -a$ is a linear extrapolation of that at the next two input stations x. As the number of computational stations is increased, so does the leading-edge pressure, and in the limit it will approach infinity as required. This modification has only a small effect on the free surface and any such effect is confined to the immediate neighbourhood of the leading edge.

Figure 8 shows a longitudinal cut along the centreline of the applied pressure distribution. One can anticipate that the x-spacing between computational stations must be very fine near the leading edge in order to capture the rapid change in pressure there, but that a similar resolution for the remainder of the rectangle is unnecessary. This can be accommodated simply by subdividing the rectangle into two patches, much as with the previous tandem-pressure case, but now with no "null" zone between them. We chose the leading patch to be only 10% of the length and the trailing one the re-

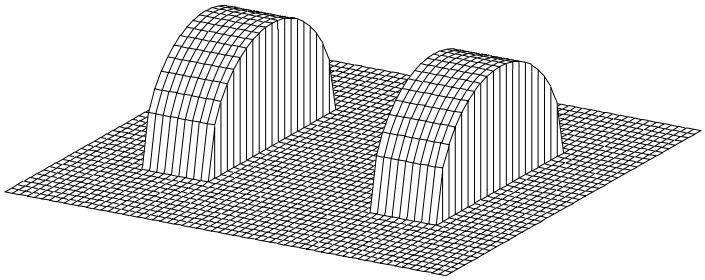

(a) Pressure distribution

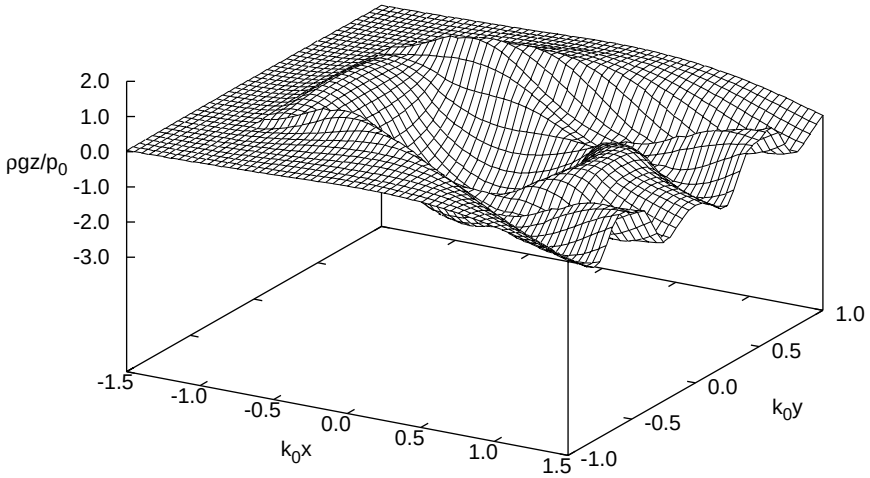

(b) Free surface

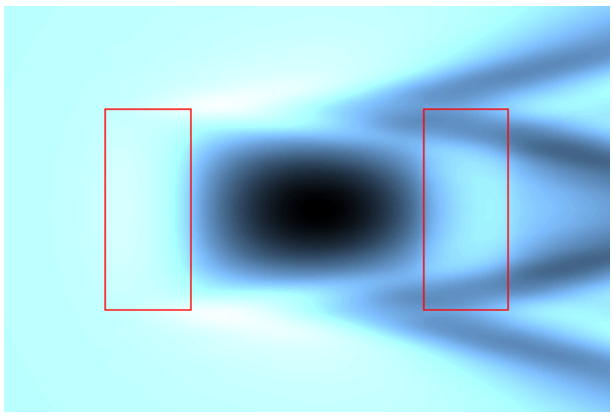

(c) Contour plot of free surface

Figure 7: Surface produced by two identical pressure patches in tandem.

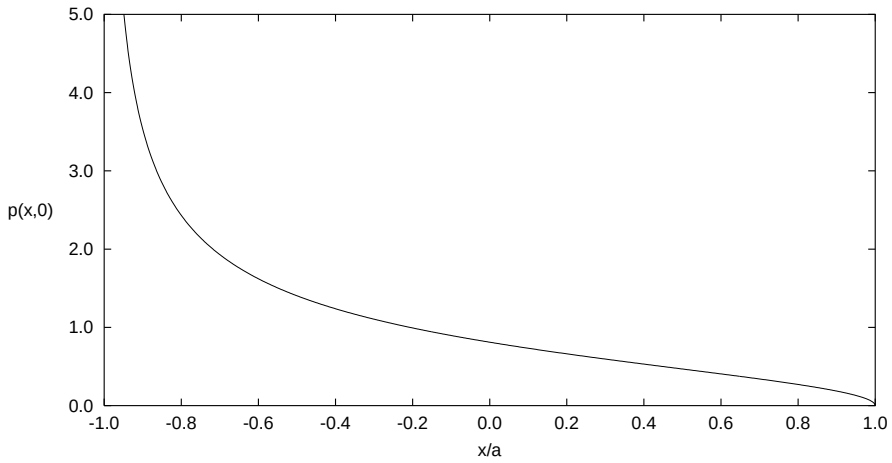

Figure 8: Longitudinal cut along the centreline of the applied pressure distribution $p(x, y) = p_1((1 - y^2/b^2)(1 - x/a)/(1 + x/a))^{1/2}$.

maining 90%, but each patch has an independent number of computational stations, thus allowing points to be concentrated near the leading edge. It is a fortunate characteristic of linear theory that the elevations due to these two patches can be computed separately and then superimposed to yield the full elevation due to the pressure (30).

Nevertheless, computing the free-surface elevation this way is an expensive numerical task, since at the leading edge the hydrostatic depression in the local-field term is very large, and must be almost cancelled by an equally large positive elevation in the far-field term. To retain reasonable accuracy in the total, both components must be determined to high accuracy, especially near the corners, where high resolution in the θ-integration of the far-field component is required.

The free-surface elevation produced by this pressure distribution is shown in Figure 9, and the region near the leading edge is shown in Figure 10. One can see clearly the extreme steepening of the free surface immediately ahead of the leading edge where, if the applied leading-edge pressure was actually infinite, the x-slope would become infinite, this being the correct linearised representation of a spray sheet. By comparison, the x-slope of the free surface within the pressure zone immediately following the leading edge is bounded and almost constant, consistent with the applied pressure being a simplifica-

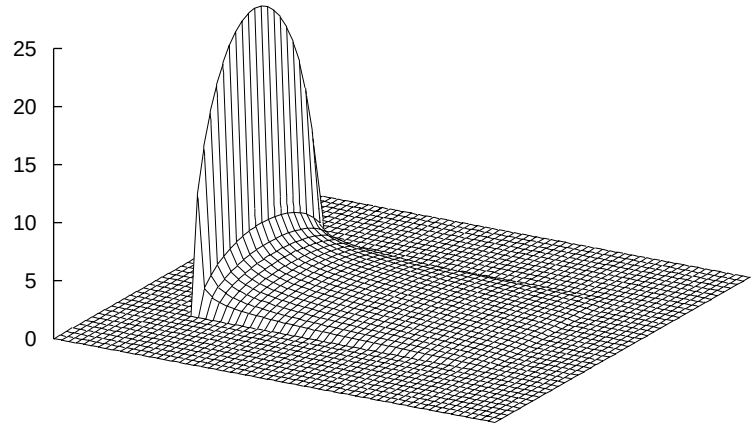

(a) Pressure distribution

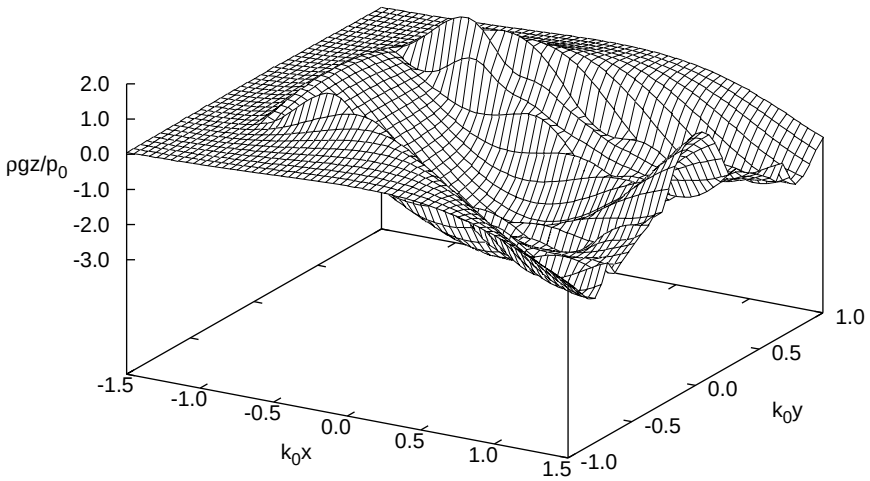

(b) Free surface

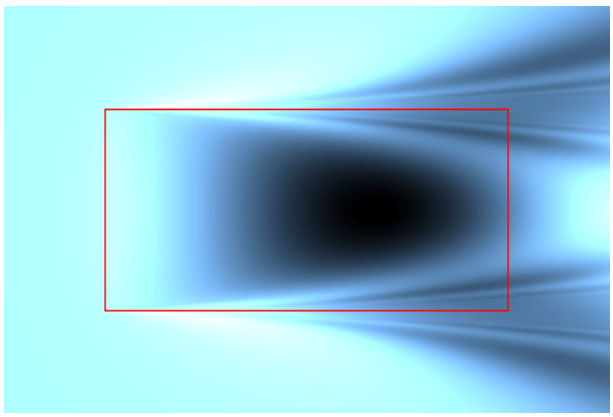

(c) Contour plot of free surface

Figure 9: Free surface due to a pressure distribution with near-singular behaviour at the leading edge.

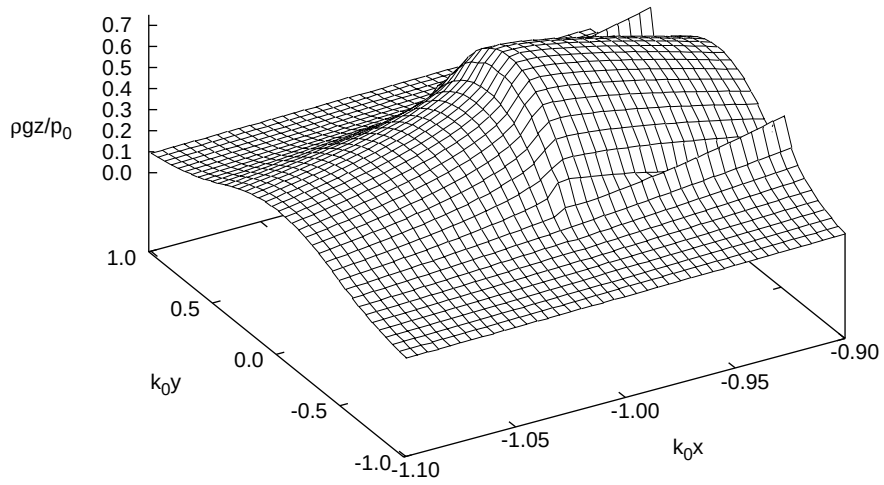

Figure 10: Near-leading-edge free surface due to a pressure distribution with near-singular behaviour at the leading edge.

tion of that due to an inclined locally-flat hull surface. Thus, it appears we are able to approximate very closely the free surface produced by pressure distributions typical of planing surfaces. With appropriate extensions to our program, we may also be able to solve the inverse problem, namely that of determining the free surface produced by a prescribed planing surface, in an accurate and efficient manner.

Acknowledgement

This work was supported by the Australian Research Council.

References

[1] Abramowitz M. and Stegun, I.E., *Handbook of Mathematical Functions*, Dover, 1964.

[2] Cheng, X. and Wellicome, J.F., *Study of planing hydrodynamics using strips of transversely variable pressure*, J. Ship Res. **38** (1994), pp. 30–41.

[3] Doctors, L.J. and Day, A.H. *Wave-free river-based air-cushion vehicles.* Proc. Intnl. Conf. Hydrodynamics of High-Speed Craft Wake Wash and Motions Control, London England, November 2000.

[4] Huang, F.T. and Wong, K.K., *Disturbance induced by a pressure distribution moving over a free surface*, J. Ship Res., Sept 1970, pp. 195–203.

[5] Lamb, H. *Hydrodynamics*, 5th edn, Cambridge 1936.

[6] Newman, J.N. *Evaluation of the wave-resistance Green function: Part 1 — The double integral.* J. Ship Res. **31** (1987) pp. 79–90.

[7] Newman, J.N. and Poole, F.A.P. *The wave resistance of a moving pressure distribution in a canal*, Schiffstechnik **9** (1962) pp. 1–6.

[8] Tuck, E.O., Scullen, D.C. and Lazauskas, L., *Ship-Wave Patterns in the Spirit of Michell.* IUTAM Symposium on Free-Surface Waves, Birmingham, July 2000. Proc. ed. Y. Shikhmurzaev, Kluwer 2001.

[9] Tuck, E.O., *Some accurate solutions of the lifting surface integral equation*, J. Austral. Math. Soc. Ser. B **35** (1993) pp. 127–144.

[10] Tuck, E.O., Collins, J.L. and Wells, W.H., *On ship waves and their spectra*, J. Ship Res. **15** (1971) pp. 11–21.

[11] Tuck, E.O. and Lazauskas, L., *Free-surface pressure distributions with minimum wave resistance*, submitted to the ANZIAM Journal (electronic), January 2001.

[12] Wehausen, J.H. and Laitone, E.H., *Surface Waves*, in Handbuch der Physik, ed. Flügge S., vol. 9. Springer-Verlag, 1962.